Electrochemical Nanoprobes for Single-Cell Analysis

ARTICLE *in* ACS NANO · DECEMBER 2013

Impact Factor: 12.88 · DOI: 10.1021/nn405612q · Source: PubMed

Electrochemical Nanoprobes for Single-Cell Analysis

Paolo Actis,[†,*] Sergiy Tokar,[†] Jan Clausmeyer,[‡] Babak Babakinejad,[†] Sofya Mikhaleva,[†] Renaud Cornut,[⊥] Yasufumi Takahashi,[§] Ainara López Córdoba,[†] Pavel Novak,[∥] Andrew I. Shevchuck,[†] Jennifer A. Dougan,[#] Sergei G. Kazarian,[#] Petr V. Gorelkin,[▽] Alexander S. Erofeev,[▽] Igor V. Yaminsky,[▽] Patrick R. Unwin,[⊗] Wolfgang Schuhmann,[‡] David Klenerman,[○] Dmitri A. Rusakov,[◆] Elena V. Sviderskaya,[×] and Yuri E. Korchev[†,*]

[†]Department of Medicine, Imperial College London, London W12 0NN, United Kingdom, [‡]Analytische Chemie-Elektroanalytik & Sensorik, Ruhr-Universität Bochum, Universitätsstrasse 150, 44801 Bochum, Germany, [§]Advanced Institute for Materials Research, Tohoku University, Sendai 980-8577, Japan, [⊥]Laboratoire de Chimie des Surfaces et Interfaces, CEA-Saclay, 91191 Gif-sur-Yvette, France, [∥]School of Engineering and Materials Science, Queen Mary, University of London, E1 4NS, United Kingdom, [#]Department of Chemical Engineering, Imperial College London, London SW7 2AZ, United Kingdom, [▽]Medical Nanotechnology, Stroiteley Strasse 4-5-47, Moscow 119311, Russia, [⊗]Department of Chemistry, University of Warwick, Coventry CV4 7AL, United Kingdom, [○]Department of Chemistry, University of Cambridge, Cambridge CB2 1EW, United Kingdom, [◆]UCL Institute of Neurology, University College London, London WC1N 3BG, United Kingdom, and [×]Division of Biomedical Sciences, St George's University of London, London SW17 0RE, United Kingdom

ABSTRACT The measurement of key molecules in individual cells with minimal disruption to the biological milieu is the next frontier in single-cell analyses. Nanoscale devices are ideal analytical tools because of their small size and their potential for high spatial and temporal resolution recordings. Here, we report the fabrication of disk-shaped carbon nanoelectrodes whose radius can be precisely tuned within the range 5—200 nm. The functionalization of the nanoelectrode with platinum allowed the monitoring of oxygen consumption outside and inside a brain slice. Furthermore, we show that nanoelectrodes of this type can be used to impale individual cells to perform electrochemical measurements within the cell with minimal disruption to cell function. These nanoelectrodes can be fabricated combined with scanning ion conductance microscopy probes, which should allow high resolution electrochemical mapping of species on or in living cells.

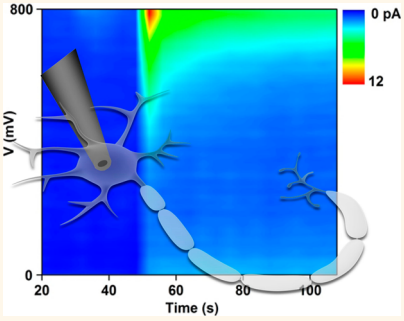

KEYWORDS: carbon · nanoelectrode · platinum · electrochemistry · intracellular measurements · brain slice · melanoma

The ability to dynamically probe individual cells within their natural environment is the next frontier in biomedicine. In particular, manipulation and analysis of individual cells with nanoscale probes should greatly enhance our understanding of processes that control the function and fate of cells. As new tools emerge, it has become apparent that the ability to assess phenotypes dynamically (*i.e.*, gene expression, protein activities, ion fluctuations, signaling) at the single cell level is key to understanding cellular behavior in a complex environment.[1−4]

Nanoscale devices are ideal single-cell surgical tools because of their potential for high spatial and temporal resolution recordings with minimal disturbance to cell functions.[5,6] Recently, two groups independently developed cellular nanoendoscopes for single cell analysis. Singhal *et al.* attached a carbon nanotube to the tip of a glass micropipet and showed its potential for interrogating cells down to the single organelle level.[7] Similarly, Yan *et al.* developed a nanowire waveguide attached to the tip of an optical fiber, to transmit visible light into the intracellular compartments of a living mammalian cell and detect optical signals from subcellular regions.[8] However, in general, intracellular measurements with nanoprobes are often limited to the monitoring of membrane potential. Lieber's group, for instance, developed a nanoscale field effect transistor (nanoFET) based on a kinked nanowire that was able to penetrate living cells and record intracellular potentials.[6] Similarly, Angle *et al.* starting from conventional tungsten microelectrodes[9] and Yoon *et al.* from a pure carbon nanotube[10] developed nanoelectrodes capable of intracellular recordings.

Historically, micro- and nanoelectrodes fabricated from carbon fibers have found vast applications in the quantitative study of exocytosis. In neuroscience research, microelectrode have been used extensively for

* Address correspondence to p.actis@imperial.ac.uk, y.korchev@imperial.ac.uk.

Received for review October 28, 2013 and accepted December 30, 2013.

Published online December 30, 2013
10.1021/nn405612q

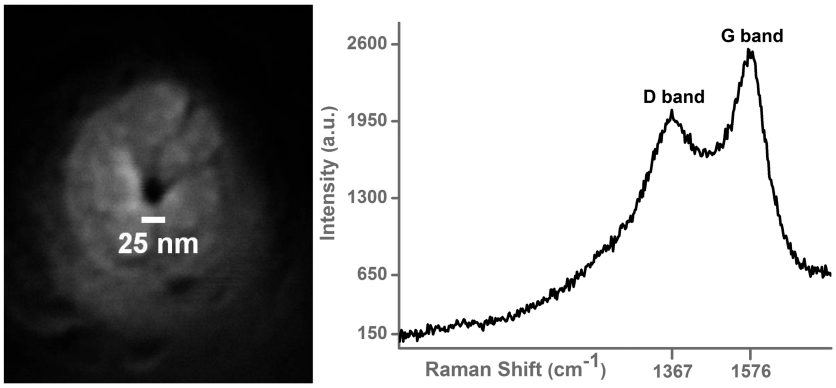

Figure 1. Physical characterization of carbon nanoelectrodes: (Left) SEM micrograph of a nanoelectrode tip coated with a thin (~10 nm) layer of Cr; (right) representative Raman spectrum of the nanoelectrode tip.

the determination of oxygen consumption, reactive oxygen and nitrogen species,[11−13] and for the analytical detection of electrochemically active neurotransmitters both *in vivo* and *in vitro*.[12,14−16] Mirkin's group pioneered the application of electrochemical probes for the measurement of redox properties of living cells.[17] Recently, a joint effort between Amatore and Mirkin's groups demonstrated the application of platinized nanoelectrodes for the intracellular detection of ROS species inside murine macrophages.[18] However, despite the nanometer dimension of the electro-active area, the outer glass coating was of several hundreds of nanometers.

Our group has been at the forefront of the integration of nanopipettes into Scanning Ion Conductance Microscopy (SICM) for high resolution topographical imaging of living cells.[19,20] Among many different applications, we recently showed the application of SICM for the quantitative delivery of molecules to the surface of living cells[21] and for nanoscale targeted patch clamp measurements in neuronal cultures.[22] Additionally, nanopipette probes still hold great promise as intracellular biosensors[23−25] and as tools for cell manipulation.[26−28] We recently developed a method to fabricate multifunctional nanoprobes starting from double-barrel quartz nanopipettes. Pyrolytic carbon is selectively deposited on one barrel while leaving the other one unchanged. We employed these nanoprobes for simultaneous SICM-SECM imaging[29] and for the measurement of the electrochemical activity of the surface of living cells.[30]

Here we describe the fabrication, characterization, and tailoring of carbon nanoelectrodes for intracellular electrochemical recordings. We demonstrate the fabrication of disk-shaped nanoelectrodes whose radius can be precisely tuned within the range 5−200 nm. The functionalization of the nanoelectrode with platinum allowed the monitoring of oxygen consumption outside and inside a brain slice. Furthermore, we show that nanoelectrodes of this type can be used to penetrate a single cell and perform electrochemical measurements within the cell with minimal disruption to cell function.

RESULTS AND DISCUSSION

Carbon nanoelectrodes were fabricated using a top-down approach, as detailed in the methods section and in the Supporting Information (SI, Figure S1). Briefly, a quartz capillary was pulled into a sharp nanopipette tip, and carbon was pyrolitically deposited within the nanopipette shaft. This procedure generated a disk-shaped carbon nanoelectrode (Figure 1) whose radius depends on the size of the nanopipette opening.

The carbon layer consisted of a graphitic network with considerable disorder, as suggested by Raman spectroscopic analysis. Raman spectroscopy is a powerful tool for analyzing carbon materials, including graphite-based systems.[31] A representative Raman spectrum with clearly resolved D and G bands at 1367 and 1576 cm^{-1} is shown in Figure 1. There is no evidence from the extended spectrum areas (not shown) of the G′ (or 2D) band in the region ~2500−2800 cm^{-1} which is observed for highly ordered graphite. This, combined with the relatively high D:G band ratio, indicates that the graphitic material produced is disordered in nature. Scanning electron microscopy (SEM) and Energy-dispersive X-ray spectroscopy (EDX) confirmed the presence of a carbon layer that extended from the tip into the internal body of the probe, for a distance of several mm, homogenously covering the nanopipette interior with a thickness of ~300 nm (Supporting Information, Figures S2 and S3).

It has proven challenging to image nanoelectrodes smaller than ~50 nm by SEM, and alternative methods of characterization have been developed.[29,30,32] In this work, the size and geometry of the carbon nanoelectrodes were estimated using electrochemical measurements and compared to simulated electrochemical data of nanoelectrodes with known geometry, an approach which gives good insight into characteristic geometry if care is taken with the measurements (*vide infra*).

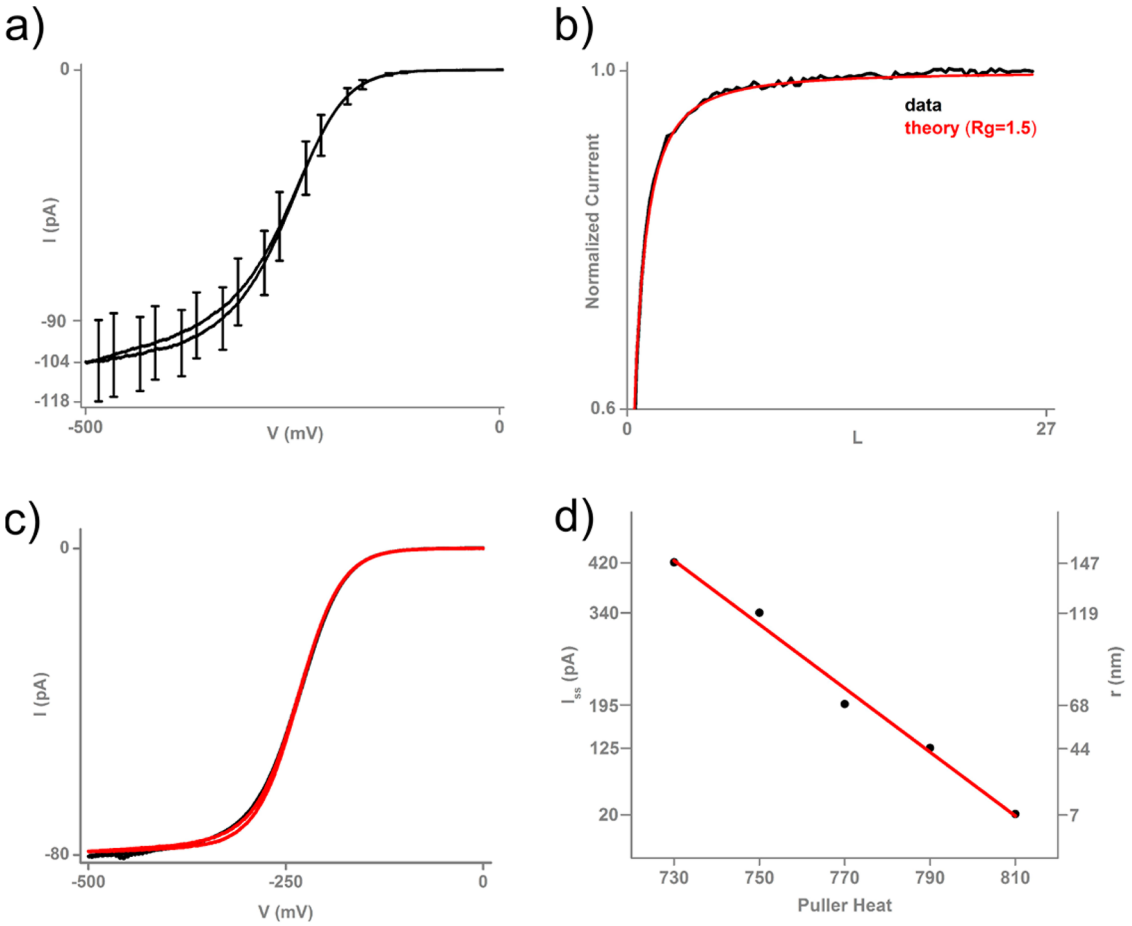

Figure 2. Electrochemical characterization of carbon nanoelectrodes. (a) Reproducibility of nanoelectrode fabrication. Average steady state current (104 ± 14) pA from measurements on 7 different electrodes, prepared using the same protocol, corresponding to an apparent radius of (30 ± 4) nm. (b) Approach curve of a representative nanoelectrode (64 nm radius) toward a polystyrene substrate. Black line, experimental data; red line, theoretical approach curve for a disk shaped electrode with R_g = 1.5. *L* is the dimensionless distance (distance divided by the nanoelectrode radius). For all experiments, the solution was 10 mM $Ru(NH_3)_6Cl_3$ in PBS. (c) Representative CVs of nanoelectrodes fabricated from twin nanopipettes (*i.e.*, the two 'mirror' nanopipettes produced in the pulling process). The overlap of the cyclic voltammograms (red and black curves) indicates minimal variability introduced by the carbon deposition, and the high level of precision achievable from the fabrication process. (d) Nanoelectrode apparent radius as a function of nanopipette pulling parameters. Black dots are experimental data extrapolated from the steady-state diffusion-limited current following eq 1; red line represents the linear fit to experimental data (R^2 = 0.986).

The parameter R_g is defined as the ratio between the overall radius of the nanoelectrode tip divided by the radius of the electrochemically active area and it can be an important parameter in interpreting the electrochemical measurements. For example, R_g has some influence on the lateral resolution when such a nanoelectrode is used for scanning electrochemical microscopy (SECM).[30] Assuming an R_g of 1.5, the apparent radius *r* of the nanoelectrode can be calculated from the steady-state current (I_{ss}) of a cyclic voltammogram by employing the expression for disk microelectrodes:

$$r = \frac{I_{ss}}{4.64nFCD} \quad (1)$$

where *n* is the number of electrons transferred in the tip reaction, *F* is the Faraday constant, *D* is the diffusion coefficient of $Ru(NH_3)_6^{3+}$ used as the redox probe (one electron reduction), and *C* is its concentration in solution (Figure 2a). This equation estimates the nanoelectrode active area, with the assumption that the nanoelectrode active element and insulating sheath are coplanar. This has to be verified by comparing simulated and experimental approach curves of the nanoelectrode to a surface of known activity, *e.g.*, for an inert polystyrene surface (Figure 2b, Supporting Information Figure S4).[33,34] The experimental data fit well to a simulated curve for a coplanar disk electrode with a radius of 64 nm and an R_g of 1.5,[35] in agreement with that estimated from the steady-state limiting current with the probe away from the surface. We performed a systematic study to investigate the reproducibility of the nanoelectrode fabrication, by preparing several nanopipettes (*N* = 7) with identical pulling parameters, deposited carbon, and averaged their steady state current extrapolated

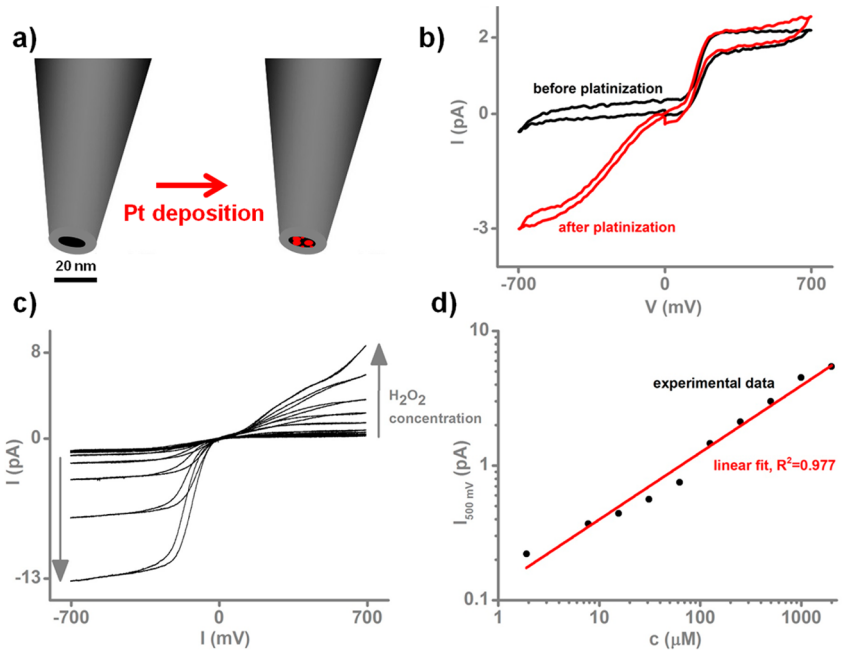

Figure 3. Functionalization of a carbon nanoelectrode with platinum and analytical detection of hydrogen peroxide. (a) Cartoon showing a carbon nanoelectrode fabricated in a single barrel nanopipette and its functionalization with platinum. (b) Cyclic voltammograms in 1 mM ferrocene methanol in PBS of a carbon nanoelectrodes (apparent radius ~5 nm) before (black curve) and after (red curve) platinization. The platinized nanoelectrode shows increased catalytic activity toward oxygen reduction. (c) Detection of the oxidation of hydrogen peroxide by the platinized carbon nanoelectrode and (d) its dose response curve.

from cyclic voltammograms. We obtained an average I_{ss} of 104 ± 14 pA which corresponds to an apparent radius of 30 ± 4 nm (Figure 2a).

The first step in the nanoelectrode fabrication is the laser pulling of the quartz nanopipette, which generates a pair of virtually identical nanopipettes. The CVs of the nanoelectrodes prepared from such a pair of nanopipettes overlap, and again give a limiting current consistent with 28 nm radius (Figure 2c, and Supporting Information Figure S5), highlighting that the pyrolytic deposition of carbon introduces minimal variability. Furthermore, the nanoelectrodes show a well-defined steady state current up to a scan rate of 500 V/s (Figure S6). All these data from different measurements confirm that this simple fabrication procedure reproducibly generates disk-shaped nanoelectrodes of tunable size.

The nanoelectrode radius can be precisely controlled by adjusting the heat delivered by the laser during the fabrication of nanopipettes. Laser pullers have five parameters that can be changed to obtain nanopipettes of desired shape and size (heat, filament, velocity, delay, and pull). Increasing the heat delivered by the laser during the pulling process generates sharper nanopipettes and, thus, after carbon deposition, smaller nanoelectrodes. In fact, there is a linear correlation between the laser heat and the final nanoelectrode size. This allows fine-tuning of the nanoelectrode radius within the range 10−150 nm (Figure 2d).

Carbon itself is a fairly inert material and to detect some redox-active species further functionalization is needed. For example, as we consider herein, an electrodeposited platinum layer enhances the electrocatalytic activity by drastically reducing the overpotential of the reduction of oxygen and the oxidation/reduction of hydrogen peroxide. Platinum deposition was carried out by sweeping the potential from 0 to −800 mV *vs* Ag/AgCl three times in a solution containing 2 mM $PtCl_6^{2-}$. The deposition of Pt only slightly increased the effective geometric surface area of the nanoelectrode (as evidenced by the voltammogram for the oxidation of 1 mM FcMeOH), but dramatically enhanced its catalytic activity toward oxygen reduction (Figure 3b).[36] We noticed that increasing the number of cycles to 10 did not cause increase the catalytic properties of the nanoelectrode toward oxygen reduction. These findings are consistent with the ones reported by Yasin *et al.* They showed that the nucleation of Pt on carbon is a very slow process with a large overpotential, which leads to surfaces with dispersed nuclei and that the nuclei grow only to a limiting volume before the growth stops.[37] Nanoelectrodes as small as 5 nm in apparent radius (Figure 3b) can be rapidly functionalized with Pt, and used as analytical sensors for oxygen and hydrogen peroxide in solution.[38] Hydrogen peroxide (H_2O_2) is a product of cellular respiration and it plays a crucial role in biological systems as a signaling molecule in regulating diverse biological processes.[39] Upon addition of H_2O_2, the cyclic voltammogram shows an increase both in cathodic and anodic current due to reduction and oxidation of H_2O_2. The anodic current at the nanoelectrode responds

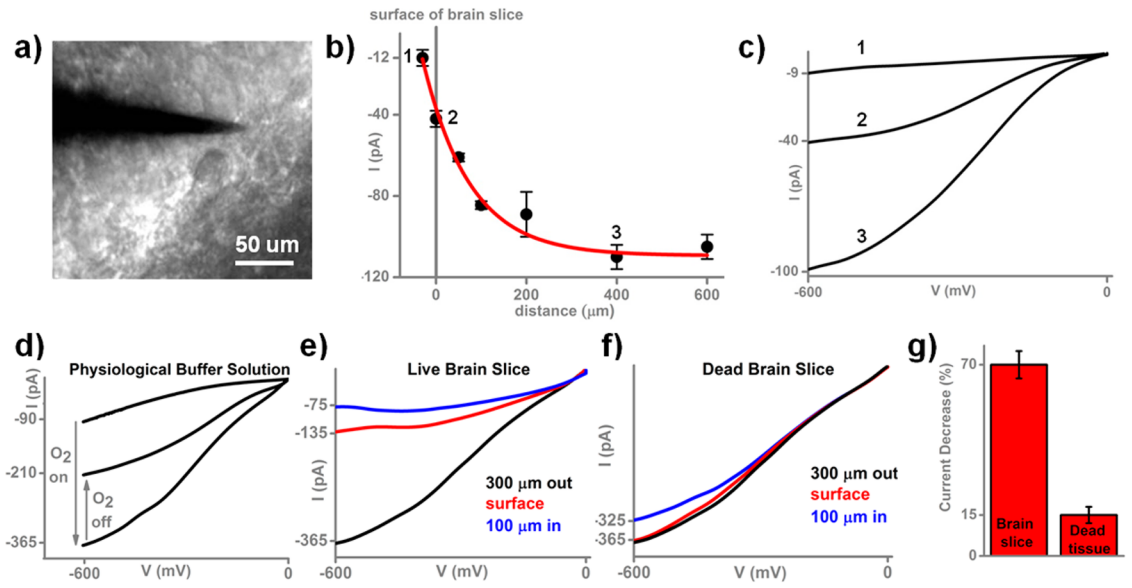

Figure 4. Oxygen measurements outside and inside a brain slice. (a) Optical micrograph of the brain slice surface (hippocampal area CA1), with cell body profiles and the carbon nanoelectrode depicted. (b) Current value at −600 mV *vs* Ag/AgCl as a function of the nanoelectrode position inside and outside the slice. (c) Voltammograms of the platinized nanoelectrode recorded at different distance from the brain slice: 1 (inside), 2 (surface), 3 (400 μm away). (d) Voltammograms of the platinized nanoelectrode immersed in physiological solution in ambient conditions (top trace), after 10 min perfusion with oxygen-saturated solution (bottom trace) and 10 min after switching off the perfusion system (middle trace). (e) Further example voltammograms of a platinized nanoelectrode at different distance from a live brain slice. (f) Voltammograms of the same platinized nanoelectrode in (e) at different distance from an oxygen-deprived brain slice. (g) Decrease of cathodic current of a platinized carbon nanoelectrode (at −600 mV *vs* Ag/AgCl) upon penetration of a healthy and oxygen-deprived brain slice. Error bars reflect the average of three measurements performed with the same nanoelectrode.

linearly to increasing concentration of hydrogen peroxide in solution (Figure 3c,d) within the biologically relevant range of 2 μM to 2 mM[40] and can be detected by both oxidation and reduction (Figure 3c). The response in the cathodic current obviously could also involve the reduction of oxygen as well from the aerated solution. However, the cathodic current in the CV amounts to −13 pA at 2 mM H_2O_2, much larger than for O_2 (*vide supra*), which indicates that the cathodic current is not solely carried by the reduction of oxygen. Moreover, Figure 3b shows that the plateau for oxygen reduction is only reached at potentials as cathodic as −600 mV whereas the plateau in Figure 3c already sets in at −200 mV. In the literature, reduction of hydrogen peroxide at platinized electrodes is observed at similar potentials.[41] The anodic response is free from complications due to oxygen and the limiting response (at 500 mV) can be seen to be linear with concentration.

Having demonstrated the ability of functionalized carbon nanoelectrodes to be used as nanosensors in solution, we next used them to monitor the oxygen consumption in acute brain slices.

Several groups reported the use of microelectrodes for mapping of oxygen consumption in isolated cells[42] and in living tissue,[43] but here we present the first use of a nanoprobe for monitoring oxygen concentration inside and outside a brain slice (three-week-old, transverse 300 μm hippocampal slices, prepared and maintained in accord with standard protocols for patch-clamp electrophysiology).[44] A platinized nanoelectrode was integrated into a home-build micromanipulator placed on an upright microscope. The nanoelectrode was polarized at −600 mV *vs* Ag/AgCl (for the diffusion-limited detection of O_2) and manually approached to the surface of the brain slice (Figure 4a). Figure 4b,c shows the decrease of the cathodic current upon approaching to the brain slice. This is due to the local depletion of oxygen caused by the respiratory activity of living neurons in the brain slice. Note that the nanoelectrode was approached and retracted (several times) over a predefined distance from a brain slice and the cathodic current − distance approach curve was found to be consistent (Figure 4b). The cathodic current dropped even further from −40 to −9 pA after insertion of the nanoelectrode into the brain slice. This decrease is not just due to hindered diffusion of O_2 within the tissue, as seen in other tissue.[45] We measured the response of a platinized nanoelectrode to the same solution (cell growth medium) with different degree of oxygenation. We measured a current of −90 pA (at −600 mV) when the nanoelectrode was immersed in the growth medium with no oxygenation. The bath solution was then constantly perfused with a solution saturated in molecular oxygen and the cathodic current increased to −365pA, which is roughly 4 times the value measured before. We then switched off the perfusion system and, after 10 min, the cathodic current decreased to −210pA. The current reached the initial value of −90 pA only when a nonoxygenated

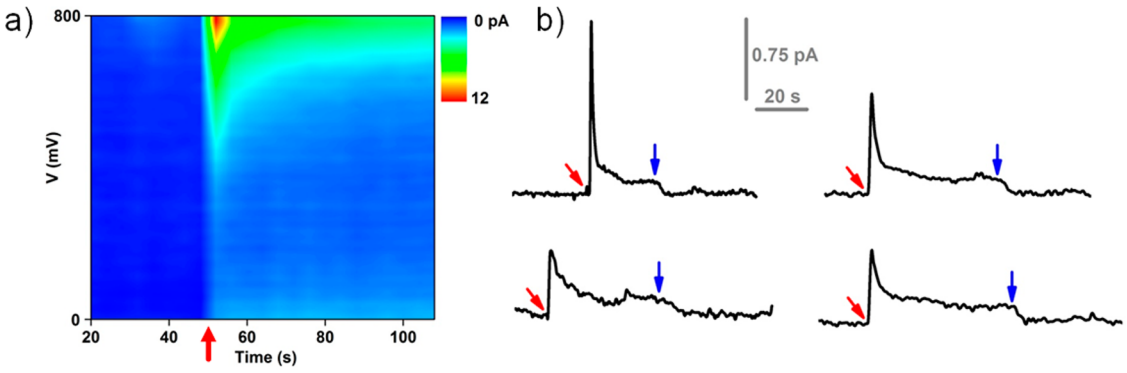

Figure 5. Intracellular measurements in individual neurons in a brain slice. (a) Background subtracted voltammograms before and after penetration of a neuron with the nanoelectrode. Voltage is applied *vs* Ag/AgCl. (b) Representative current traces of a nanoelectrode polarized at +850 *vs* Ag/AgCl inside and outside a neuron. Red and blue arrows indicated, respectively, the moment of penetration and retraction. The four traces were obtained from four different cells using the same nanoelectrode.

solution was perfused. With the same nanoelectrode, we measured the dependence of the cathodic current to the distance from a live (figure 4e) and oxygen-deprived ("dead", Figure 4f) brain slice. The cathodic current decreases from −365 pA (in the bulk solution) to −135 pA in proximity of the surface of the live brain slice, while no difference was detected close to a dead brain slice. The electrode current decreases even further when placed inside the slice, with a clear difference between the live and oxygen-deprived tissue (Figure 4g). Because the decrease in the O_2 current in the tissue is consequent to metabolic activity, these findings suggest the utility of these functional nanoprobes to monitor oxygen-dependent activity in brain slices. Also, the nanometer size of the nanoelectrode allows measurement of oxygen consumption deep inside the brain slice with minimal damage and perturbation to the biological milieu. Platinized nanoelectrodes were recently used for the intracellular detection of Reactive Oxygen and Nitrogen species (ROS/RNS) species inside murine macrophages.[18] In that work, despite the nanometer dimension of the electro-active area, the outer glass coating was of several hundreds of nanometers. The small outer diameter of our nanoelectrodes allowed us to perform electrochemical measurement both in tissue and in cultured cells at the single-cell level. The nanoelectrode can be precisely inserted into an individual neuron within the brain slice to monitor intracellular molecules. Cyclic voltammograms were measured continuously at 400 mV/s as the nanoelectrode was manually approached to the neuron of interest. Figure 5a is a background subtracted 3D plot that shows the anodic scan as a function of time. At the moment of penetration (at around 50s) a sudden increase in the anodic current is elicited at potentials in the range 500−850 mV. Amatore and co-workers explained such increase as enhanced production of ROS/RNS caused by the mechanical damage to the cell membrane.[11]

Interestingly, chronoamperometry measurements (with the nanoelectrode poised at a potential of 850 mV) during the penetration of individual neurons within the brain slice always elicited a similar signal: a quick (0.1 s) increase in current followed by a relatively slow decrease and equilibration (5 s) to a current value well above the one measured outside the neuron (Figure 5b). The current quickly goes back to baseline upon retraction of the nanoprobe from the cell cytoplasm (Figure 5b). The penetration of 5 different neurons with the same nanoelectrode generated a reproducible intracellular anodic current 100 fA above the baseline (Figure S7). None of these signals are related to the value of the cell membrane potential.[46,47] Even after depolarization of the cell membrane we detected the same signals (data not shown). We interpret this value as the measurement of flux of endogenous intracellular molecules to the nanoelectrode.

Furthermore, we applied this type of nanoelectrodes to intracellular measurements in cultured melanoma cells (Figure 6a). Melanoma is a very aggressive skin cancer which causes significant structural modification of melanosomes, organelles containing light-absorbing pigments responsible for the scavenging of free radicals. Melanosomes found in melanomas, instead of protecting the cell from oxidative stress, produce free radicals.[48] Figure 6b shows that upon penetration of the melanoma cells the anodic current quickly increases followed by equilibration to a level above the one measured in the cell media (Figure 6c). A cell can withstand multiple penetrations and the value of anodic current measured inside the cell is consistent even after repeated penetrations/retractions. Interestingly, we observed a relatively large spike in current only for the very first cell penetration while for successive penetrations the spike was either diminished or not present at all. This may suggest a correlation between the initial current spike and the mechanical damage caused to the cell by penetration with the nanoelectrode. We believe these results show the potential of functional nanoelectrodes to probe endogenous species in melanoma cells and they may allow

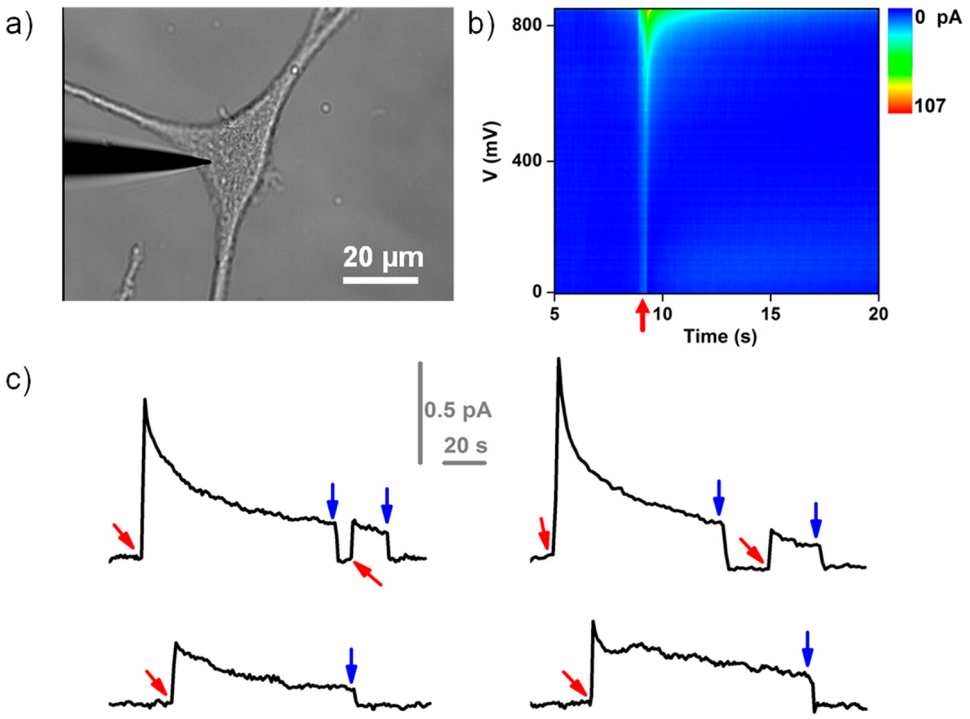

Figure 6. Intracellular measurements in melanoma cells. (a) Optical micrograph of a nanoelectrode about to penetrate a melanoma cell. (b) Background subtracted voltammograms before and after penetration of a melanoma cell with the nanoelectrode. Voltage is applied *vs* Ag/AgCl. (c) Representative current traces of a nanoelectrode polarized at +850 mV *vs* Ag/AgCl inside and outside a melanoma cell in culture. Red and blue arrows indicated, respectively, the moment of penetration and retraction. The four traces were obtained from four different cells using the same nanoelectrode.

the study of oxidative stress in melanomas. Current research in our group is oriented toward the application of surface chemistry for the detection of ROS at more moderate potential (*e.g.*, −50 mV).[49]

We briefly mention that the nanoelectrodes we have described have the potential to be integrated into multifunctional nanoprobes. Starting from double barrel nanopipettes, one can selectively deposit carbon on either one[29] or both barrels.[50] The nanoelectrodes formed in this way can be independently functionalized with platinum (Figure S8). Unmodified barrels, filled with electrolyte solution, can be used for SICM distance control. This channel allows the positioning of nanoprobes with subcellular resolution and would allow the mapping of oxygen consumption outside living cell[42] or the functional study of mitochondrial respiration.[51]

CONCLUSIONS

Here, we have demonstrated a method to fabricate carbon nanoelectrodes whose radius can be precisely tuned within 5−200 nm. Nanoelectrodes can be functionalized using established electrochemical methods and we showed for the first time their application for functional measurement of metabolic activity inside brain slices. The use of nanoelectrodes minimizes the perturbation to the tissue because oxygen depletion is reduced by their small area. Furthermore, the nanoelectrodes can be precisely inserted into individual cells both in tissue and in isolated cells to perform intracellular electrochemical measurements. The application of these nanoelectrodes is by no mean limited to biological measurements and we envision their application in the emerging field of nanoscale interfacial science.[52,53]

MATERIALS AND METHODS

Chemicals. Hexaammineruthenium(III) chloride ($Ru(NH_3)_6Cl_3$; Sigma-Aldrich) and ferrocene methanol (Sigma-Aldrich) were used as the redox species for electrode characterization. Phosphate buffered saline (PBS) solution was prepared from 7.2 mM Na_2HPO_4, 2.8 mM KH_2PO_4, and 150 mM NaCl (pH 7.4).

Nanoelectrode Fabrication. The fabrication comprised two steps: the laser pulling of a quartz capillary into a nanopipette, and the filling of the nanopipette tip with pyrolitic carbon (Figure S1).

Nanopipette Fabrication. Nanopipettes were fabricated using a P-2000 laser puller (Sutter Instrument) from quartz capillaries with an outer diameter of 1.2 mm and an inner diameter of 0.90 mm (Q120-90-7.5; Sutter Instrument). Parameters used mainly (for 30 nm radius nanoelectrodes) were the following: heat 790, filament 3, velocity 45, delay 130, and pull 90, although the 'heat' parameter was varied to assess the effect on nanoelectrode size.

Deposition of Pyrolytic Carbon. The nanopipette was filled with butane gas *via* tygon tubing. A butane jet flame torch lighter was used to deposit pyrolytic carbon inside the nanopipette taper. The reaction has to be performed within an inert atmosphere to prevent etching of the deposited carbon layer. Photographs of all the different steps in nanoelectrode

fabrication can be found in the Supporting Information. The entire fabrication process takes on average less than a minute per nanoelectrode.[29] The fabrication process is similar to the one described by Kim *et al.*, but it produces disk shaped nanoelectrodes instead of carbon-ring electrodes.[54] Amemiya's group showed that nanoelectrodes can be damaged by electrostatic discharge.[55] In this work we never observed any apparent damage during the fabrication and handling of the nanoelectrodes.

Platinization of Carbon Nanoelectrodes. Carbon nanoelectrodes are platinized in a solution of chloroplatinic acid H_2PtCl_6 (2 mM) in 0.1 hydrochloric acid. The reduction of Pt at the carbon nanoelectrode was induced *via* cyclic voltammetry from 0 to −800 mV with a scan rate of 200 mV/s.

Cyclic Voltammetry. The nanoelectrode was back contacted with a silver wire and immersed into a solution of 10 mM hexaammineruthenium(III) chloride or 1 mM ferrocene methanol in PBS. An Ag/AgCl electrode was placed in a 2 mL of bulk solution acting as an auxiliary/reference electrode. All potentials are quoted against this electrode. Both electrodes were connected to an Axopatch 700B amplifier with the DigiData 1322A digitizer (Molecular Devices), and a PC equipped with pClamp 10 software (Molecular Devices). All measurements were performed at room temperature.

SECM Setup. The SECM instrument was similar to that previously described and operated in hopping mode.[30] The Faradaic current was measured with a MultiClamp700B patch-clamp amplifier (Axon Instruments). The electrochemical signal was filtered using a low-pass filter at 1000 Hz and digitized with an Axon Digidata 1322A (Axon Instruments). To record approach curves, the set-point was maintained at 80% of the steady-state current measured in bulk solution (I_{ss}). The scan head of the SECM instrument consisted of a PIHera P-621.2 XY Nanopositioning Stage (Physik Instrumente (PI), Germany) with 100 × 100 μm travel range that moved the sample and a LISA piezo actuator P-753.21C (PI, Germany) with travel range 25 μm for pipet positioning along the *Z*-axis. Coarse positioning was achieved with translation stages M-111.2DG (*XY* directions) and M-112.1DG (*Z*-axis) (PI, Germany). Piezo actuators were powered by high voltage amplifiers E-503 and E-505 (PI, Germany) and a servo module E-509 (PI, Germany) operating in closed-loop. The setup was controlled using software written in Delphi (Borland) and Code Composer Studio (Texas Instruments) for a ScanIC controller (Ionscope).

SEM Imaging. SEM imaging was performed with a Zeiss Auriga equipped with a field emission gun. Accelerating voltage was set to 5 kV. Samples were coated with a ~5 nm layer of Cr before imaging using a sputter coater.

Raman Spectroscopy. Raman spectra were collected from microelectrodes, prepared in the same fashion as the nanoelectrodes. The carbon microelectrodes were fixed, horizontally, on a coverslip with the laser carefully focused at the end of the tip from where the Raman spectra were acquired. Raman measurements were performed using a Renishaw 1000 confocal Raman microspectrometer using an Ar-ion laser, 514 nm, *via* a 50× objective (NA = 0.75) and Peltier-cooled CCD detector. The spectra were acquired with 1 s × 100 accumulations with a maximum output laser power of 20 mW.

Brain Slices Preparation. Hippocampus slices were isolated from 28 days old rats using standard, long established techniques.[56] After decapitation of the rats was performed, the rat brain was isolated and placed into ice-cold ringer solution, where the hippocampus isolation was performed. The hippocampus was sliced into 350-μm-thick transverse slices, using a Leica VT1200S blade microtome. After obtaining the cut slices, we stored them in the same solution at 34 °C for 15 min. Then they were stored for at least 1 h at room temperature. During and after isolation, the solution was constantly bubbled with a 95% O_2 and 5% CO_2 gas mixture.

Melanoma Cells Preparation. Human melanoma line, A375P, was grown in RPMI 1640 medium (Invitrogen, Paisley, Renfrewshire, U.K.) supplemented with fetal calf serum (10%, Invitrogen), L-glutamine (2 mM, Invitrogen), penicillin/streptomycin (100 U/mL and 100 μg/mL, respectively, Sigma, Gillingham, Dorset, U.K.) and phenol red (7.5 μg/mL, Sigma) at 37 °C with 10% CO_2. Normal human melanocyte line was grown as above with the addition of 200 nM 12-*O*-tetradecanoyl phorbol 13-acetate (Sigma), 200 pM cholera toxin (Sigma), 10 ng/mL human stem cell factor (Invitrogen) and 10 nM endothelin 1 (Bachem). The cells were obtained from the Functional Genomics Cell Bank at St George's.[57]

Conflict of Interest: The authors declare no competing financial interest.

Acknowledgment. This work was funded by the EPSRC and by Wellcome Trust. We acknowledge Dr. M Ardakani for assistance in SEM imaging. P.V.G., A.S.E., and I.V.Y. thank the Ministry of Education and Science of the Russian Federation Contract No. 14.512.11.0084. P.R.U. thanks the European Research Council for an Advanced Investigator grant (ERC-2009-AdG 247143 "QUANTIF"). R.C. thanks Programme Retour Post-Doctorants (ANRPDOC20011-Copel) for funding.

Supporting Information Available: Photographs of nanoelectrode fabrication; SEM micrographs and EDX analysis of nanoelectrodes. Reproducibility of nanoelectrode fabrication; cyclic voltammetry of a carbon nanoelectrode at different scan rates. Intracellular detection with a platinized carbon nanoelectrode; platinization of double-barrel carbon nanoelectrode. This material is available free of charge *via* the Internet at http://pubs.acs.org.

REFERENCES AND NOTES

1. Schubert, C. Single-Cell Analysis: The Deepest Differences. *Nature* **2011**, *480*, 133–137.
2. Wang, D.; Bodovitz, S. Single Cell Analysis: The New Frontier in 'Omics'. *Trends Biotechnol.* **2010**, *28*, 281–290.
3. Zheng, X. T.; Li, C. M. Single Cell Analysis at the Nanoscale. *Chem. Soc. Rev.* **2012**, *41*, 2061–2071.
4. Trouillon, R.; Passarelli, M. K.; Wang, J.; Kurczy, M. E.; Ewing, A. G. Chemical Analysis of Single Cells. *Anal. Chem.* **2012**, *85*, 522–542.
5. Yum, K.; Wang, N.; Yu, M.-F. Nanoneedle: A Multifunctional Tool for Biological Studies in Living Cells. *Nanoscale* **2010**, *2*, 363–372.
6. Tian, B.; Cohen-Karni, T.; Qing, Q.; Duan, X.; Xie, P.; Lieber, C. M. Three-Dimensional, Flexible Nanoscale Field-Effect Transistors as Localized Bioprobes. *Science* **2010**, *329*, 830–834.
7. Singhal, R.; Orynbayeva, Z.; Kalyana Sundaram, R. V.; Niu, J. J.; Bhattacharyya, S.; Vitol, E. A.; Schrlau, M. G.; Papazoglou, E. S.; Friedman, G.; Gogotsi, Y. Multifunctional Carbon-Nanotube Cellular Endoscopes. *Nat. Nanotechnol.* **2011**, *6*, 57–64.
8. Yan, R.; Park, J.-H.; Choi, Y.; Heo, C.-J.; Yang, S.-M.; Lee, L. P.; Yang, P. Nanowire-Based Single-Cell Endoscopy. *Nat. Nanotechnol.* **2012**, *7*, 191–196.
9. Angle, M. R.; Schaefer, A. T. Neuronal Recordings with Solid-Conductor Intracellular Nanoelectrodes (SCINEs). *PLoS One* **2012**, *7*, e43194.
10. Yoon, I.; Hamaguchi, K.; Borzenets, I. V.; Finkelstein, G.; Mooney, R.; Donald, B. R. Intracellular Neural Recording with Pure Carbon Nanotube Probes. *PLoS One* **2013**, *8*, e65715.
11. Amatore, C.; Arbault, S.; Bouton, C.; Coffi, K.; Drapier, J.-C.; Ghandour, H.; Tong, Y. Monitoring in Real Time with a Microelectrode the Release of Reactive Oxygen and Nitrogen Species by a Single Macrophage Stimulated by its Membrane Mechanical Depolarization. *ChemBioChem* **2006**, *7*, 653–661.
12. Wightman, R. M. Probing Cellular Chemistry in Biological Systems with Microelectrodes. *Science* **2006**, *311*, 1570–1574.
13. Bedioui, F.; Trevin, S.; Devynck, J. Chemically Modified Microelectrodes Designed for the Electrochemical Determination of Nitric Oxide in Biological Systems. *Electroanalysis* **1996**, *8*, 1085–1091.
14. Cahill, P. S.; Walker, Q. D.; Finnegan, J. M.; Mickelson, G. E.; Travis, E. R.; Wightman, R. M. Microelectrodes for the Measurement of Catecholamines in Biological Systems. *Anal. Chem.* **1996**, *68*, 3180–3186.

15. Ariansen, J. L.; Heien, M. L. A. V.; Hermans, A.; Phillips, P. E. M.; Hernadi, I.; Bermudez, M.; Schultz, W.; Wightman, R. M. Monitoring Extracellular pH, Oxygen, and Dopamine During Reward Delivery in the Striatum of Primates. *Front. Behav. Neurosci.* **2012**, *6* (36), 1–10.
16. Chen, T. K.; Lau, Y. Y.; Wong, D. K. Y.; Ewing, A. G. Pulse Voltammetry in Single Cells Using Platinum Microelectrodes. *Anal. Chem.* **1992**, *64*, 1264–1268.
17. Sun, P.; Laforge, F. O.; Abeyweera, T. P.; Rotenberg, S. A.; Carpino, J.; Mirkin, M. V. Nanoelectrochemistry of Mammalian Cells. *Proc. Natl. Acad. Sci. U.S.A.* **2008**, *105*, 443–448.
18. Wang, Y.; Noël, J.-M.; Velmurugan, J.; Nogala, W.; Mirkin, M. V.; Lu, C.; Guille Collignon, M.; Lemaître, F.; Amatore, C. Nanoelectrodes for Determination of Reactive Oxygen and Nitrogen Species Inside Murine Macrophages. *Proc. Natl. Acad. Sci. U.S.A.* **2012**, *109*, 11534–11539.
19. Novak, P.; Li, C.; Shevchuk, A. I.; Stepanyan, R.; Caldwell, M.; Hughes, S.; Smart, T. G.; Gorelik, J.; Ostanin, V. P.; Lab, M. J.; *et al.* Nanoscale Live-Cell Imaging Using Hopping Probe Ion Conductance Microscopy. *Nat Meth* **2009**, *6*, 279–281.
20. Korchev, Y. E.; Bashford, C. L.; Milovanovic, M.; Vodyanoy, I.; Lab, M. J. Scanning Ion Conductance Microscopy of Living Cells. *Biophys. J.* **1997**, *73*, 653–658.
21. Babakinejad, B.; Jönsson, P.; López Córdoba, A.; Actis, P.; Novak, P.; Takahashi, Y.; Shevchuk, A.; Anand, U.; Anand, P.; Drews, A.; *et al.* Local Delivery of Molecules from a Nanopipette for Quantitative Receptor Mapping on Live Cells. *Anal. Chem.* **2013**, *85*, 9333–9342.
22. Novak, P.; Gorelik, J.; Vivekananda, U.; Shevchuk, A. I.; Ermolyuk, Y. S.; Bailey, R. J.; Bushby, A. J.; Moss, G. W. J.; Rusakov, D. A.; Klenerman, D.; *et al.* Nanoscale-Targeted Patch-Clamp Recordings of Functional Presynaptic Ion Channels. *Neuron* **2013**, *79*, 1067–1077.
23. Actis, P.; Mak, A.; Pourmand, N. Functionalized Nanopipettes: Toward Label-Free, Single Cell Biosensors. *Bioanal. Rev.* **2010**, *1*, 177–185.
24. Chen, C.-C.; Zhou, Y.; Baker, L. A. Scanning Ion Conductance Microscopy. *Ann. Rev. Anal. Chem.* **2012**, *5*, 207–228.
25. Morris, C. A.; Friedman, A. K.; Baker, L. A. Applications of Nanopipettes in the Analytical Sciences. *Analyst* **2010**, *135*, 2190–2202.
26. Seger, R. A.; Penfold, C.; Actis, P.; Maalouf, M.; Vilzony, B.; Pourmand, N. A Voltage Controlled Nano-Injection System for Single-Cell Surgery. *Nanoscale* **2012**, *4*, 5843–5846.
27. Brennan, L. D.; Roland, T.; Morton, D. G.; Fellman, S. M.; Chung, S.; Soltani, M.; Kevek, J. W.; McEuen, P. M.; Kemphues, K. J.; Wang, M. D. Small Molecule Injection into Single-Cell *C. elegans* Embryos *via* Carbon-Reinforced Nanopipettes. *PLoS One* **2013**, *8*, e75712.
28. Actis, P.; Maalouf, M.; Kim, H. J.; Lohith, A.; Vilozny, B.; Seger, R. A.; Pourmand, N. Compartmental Genomics in Living Cells Revealed by Single-Cell Nanobiopsy. *ACS Nano* **2013**, 10.1021/nn405097u.
29. Takahashi, Y.; Shevchuk, A. I.; Novak, P.; Zhang, Y.; Ebejer, N.; Macpherson, J. V.; Unwin, P. R.; Pollard, A. J.; Roy, D.; Clifford, C. A.; Shiku, H.; Matsue, T.; Klenerman, D.; Korchev, Y. E. Multifunctional Nanoprobes for Nanoscale Chemical Imaging and Localized Chemical Delivery at Surfaces and Interfaces. *Angew. Chem., Int. Ed.* **2011**, *50*, 9638–9642.
30. Takahashi, Y.; Shevchuk, A. I.; Novak, P.; Babakinejad, B.; Macpherson, J.; Unwin, P. R.; Shiku, H.; Gorelik, J.; Klenerman, D.; Korchev, Y. E.; *et al.* Topographical and Electrochemical Nanoscale Imaging of Living Cells Using Voltage-Switching Mode Scanning Electrochemical Microscopy. *Proc. Natl. Acad. Sci. U.S.A.* **2012**, *109*, 11540–11545.
31. Pimenta, M. A.; Dresselhaus, G.; Dresselhaus, M. S.; Cancado, L. G.; Jorio, A.; Saito, R. Studying Disorder in Graphite-Based Systems by Raman Spectroscopy. *Phys. Chem. Chem. Phys.* **2007**, *9*, 1276–1290.
32. Nogala, W.; Velmurugan, J.; Mirkin, M. V. Atomic Force Microscopy of Electrochemical Nanoelectrodes. *Anal. Chem.* **2012**, *84*, 5192–5197.
33. Mirkin, M. V.; Fan, F.-R. F.; Bard, A. J. Scanning Electrochemical Microscopy Part 13. Evaluation of the Tip Shapes of Nanometer Size Microelectrodes. *J. Electroanal. Chem.* **1992**, *328*, 47–62.
34. Cornut, R.; Lefrou, C. A Unified New Analytical Approximation for Negative Feedback Currents with a Microdisk SECM Tip. *J. Electroanal. Chem.* **2007**, *608*, 59–66.
35. Cornut, R.; Bhasin, A.; Lhenry, S.; Etienne, M.; Lefrou, C. Accurate and Simplified Consideration of the Probe Geometrical Defaults in Scanning Electrochemical Microscopy: Theoretical and Experimental Investigations. *Anal. Chem.* **2011**, *83*, 9669–9675.
36. Chen, S.; Kucernak, A. Electrocatalysis under Conditions of High Mass Transport Rate: Oxygen Reduction on Single Submicrometer-Sized Pt Particles Supported on Carbon. *J. Phys. Chem. B* **2004**, *108*, 3262–3276.
37. Yasin, H. M.; Denuault, G.; Pletcher, D. Studies of the Electrodeposition of Platinum Metal from a Hexachloroplatinic Acid Bath. *J. Electroanal. Chem.* **2009**, *633*, 327–332.
38. Pletcher, D.; Sotiropoulos, S. A Study of Cathodic Oxygen Reduction at Platinum Using Microelectrodes. *J. Electroanal. Chem.* **1993**, *356*, 109–119.
39. Halliwell, B.; Gutteridge, J. M. C. *Free Radicals in Biology and Medicine*, 3rd ed.; Oxford University Press Inc.: New York, 1999.
40. Chen, W.; Cai, S.; Ren, Q.-Q.; Wen, W.; Zhao, Y.-D. Recent Advances in Electrochemical Sensing for Hydrogen Peroxide: a Review. *Analyst* **2012**, *137*, 49–58.
41. Evans, S. A. G.; Elliott, J. M.; Andrews, L. M.; Bartlett, P. N.; Doyle, P. J.; Denuault, G. Detection of Hydrogen Peroxide at Mesoporous Platinum Microelectrodes. *Anal. Chem.* **2002**, *74*, 1322–1326.
42. Nebel, M.; Grutzke, S.; Diab, N.; Schulte, A.; Schuhmann, W. Microelectrochemical Visualization of Oxygen Consumption of Single Living Cells. *Faraday Discuss.* **2013**, *164*, 19–32.
43. Mulkey, D. K.; Henderson, R. A.; Olson, J. E.; Putnam, R. W.; Dean, J. B. Oxygen Measurements in Brain Stem Slices Exposed to Normobaric Hyperoxia and Hyperbaric Oxygen. *J. Appl. Physiol.* **2001**, *90*, 1887–1899.
44. Sylantyev, S.; Savtchenko, L. P.; Niu, Y.-P.; Ivanov, A. I.; Jensen, T. P.; Kullmann, D. M.; Xiao, M.-Y.; Rusakov, D. A. Electric Fields Due to Synaptic Currents Sharpen Excitatory Transmission. *Science* **2008**, *319*, 1845–1849.
45. Gonsalves, M.; Barker, A. L.; Macpherson, J. V.; Unwin, P. R.; O Hare, D.; Winlove, C. P. Scanning Electrochemical Microscopy as a Local Probe of Oxygen Permeability in Cartilage. *Biophys. J.* **2000**, *78*, 1578–1588.
46. Schrlau, M. G.; Dun, N. J.; Bau, H. H. Cell Electrophysiology with Carbon Nanopipettes. *ACS Nano* **2009**, *3*, 563–568.
47. Hu, K.; Gao, Y.; Wang, Y.; Yu, Y.; Zhao, X.; Rotenberg, S.; Gökmeşe, E.; Mirkin, M.; Friedman, G.; Gogotsi, Y. Platinized Carbon Nanoelectrodes As Potentiometric and Amperometric SECM Probes. *J. Solid State Electrochem* **2013**, 1–7.
48. Fruehauf, J. P.; Trapp, V. Reactive Oxygen Species: An Achilles' Heel of Melanoma? *Expert Rev. Anticancer Ther.* **2008**, *8*, 1751–1757.
49. Clausmeyer, J.; Actis, P.; López Córdoba, A.; Korchev, Y. E.; Schuhmann, W. Nanosensors for the Detection of Hydrogen Peroxide. *Electrochem. Commun.* **2014**, *40*, 28–30.
50. McKelvey, K.; Nadappuram, B. P.; Actis, P.; Takahashi, Y.; Korchev, Y. E.; Matsue, T.; Robinson, C.; Unwin, P. R. Fabrication, Characterization, and Functionalization of Dual Carbon Electrodes as Probes for Scanning Electrochemical Microscopy (SECM). *Anal. Chem.* **2013**, *85*, 7519–7526.
51. Marcu, R.; Rapino, S.; Trinei, M.; Valenti, G.; Marcaccio, M.; Pelicci, P. G.; Paolucci, F.; Giorgio, M. Electrochemical Study of Hydrogen Peroxide Formation in Isolated Mitochondria. *Bioelectrochemistry* **2012**, *85*, 21–28.
52. Oja, S. M.; Wood, M.; Zhang, B. Nanoscale Electrochemistry. *Anal. Chem.* **2012**, *85*, 473–486.
53. Lemay, S. G.; Kang, S.; Mathwig, K.; Singh, P. S. Single-Molecule Electrochemistry: Present Status and Outlook. *Acc. Chem. Res.* **2012**, *46*, 369–377.

54. Kim, Y. T.; Scarnulis, D. M.; Ewing, A. G. Carbon-Ring Electrodes with 1 μm Tip Diameter. *Anal. Chem.* **1986**, *58*, 1782–1786.
55. Nioradze, N.; Chen, R.; Kim, J.; Shen, M.; Santhosh, P.; Amemiya, S. Origins of Nanoscale Damage to Glass-Sealed Platinum Electrodes with Submicrometer and Nanometer Size. *Anal. Chem.* **2013**, *85*, 6198–6202.
56. Teyler, T. J. Brain Slice Preparation: Hippocampus. *Brain Res. Bull.* **1980**, *5*, 391–403.
57. The Wellcome Trust. The Wellcome Trust Functional Genomics Cell Bank: Holdings. *Pigm. Cell Melanoma Res.* **2010**, *23*, 147-150.